Cu_2Se-based thermoelectric cellular architectures for efficient and durable power generation

Seungjun Choo[1†], Faizan Ejaz[2†], Hyejin Ju[1], Fredrick Kim[1], Jungsoo Lee[1], Seong Eun Yang[1], Gyeonghun Kim[3], Hangeul Kim[1], Seungki Jo[1], Seongheon Baek[1], Soyoung Cho[1], Ju-Young Kim[1], Sangjoon Ahn[3], Han Gi Chae[1*], Beomjin Kwon[2*], and Jae Sung Son[1,4*]

[1]*Department of Materials Science and Engineering, Ulsan National Institute of Science and Technology (UNIST), Ulsan 44919, Republic of Korea.*

[2]*School for Engineering of Matter, Transport and Energy, Arizona State University, Tempe, AZ 85287, USA*

[3]*Department of Nuclear Engineering, Ulsan National Institute of Science and Technology, Ulsan 44919, Republic of Korea*

[4]*Center for Future Semiconductor Technology (FUST), Ulsan National Institute of Science and Technology (UNIST), Ulsan 44919, Republic of Korea*

[†]*These authors contributed equally to this work.*

* Correspondence to: hgchae@unist.ac.kr (H.G.C.), kwon@asu.edu (B.K.) and jsson@unist.ac.kr (J.S.S.)

This supplement contains

Supplementary Figures 1-14

Supplementary Table 1

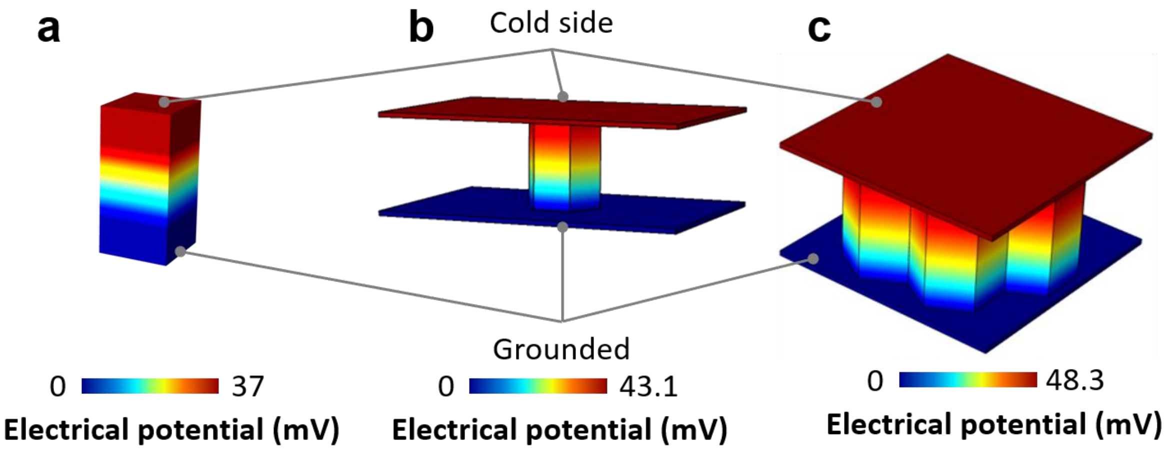

Supplementary Fig. 1 Simulated electrical potential distributions of (a) cuboid-, (b) hollow hexagonal column-, and (c) honeycomb-shaped Cu_2Se TE legs.

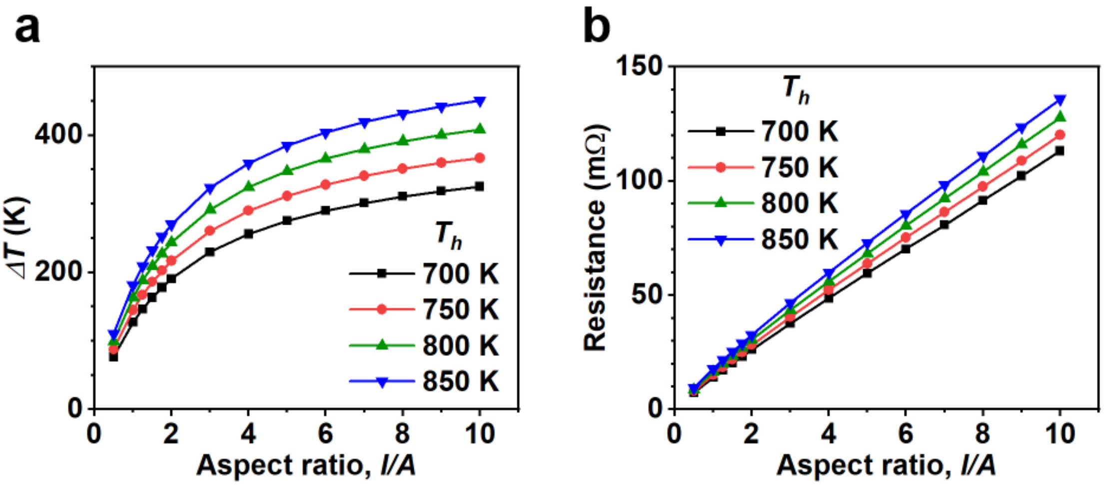

Supplementary Fig. 2 Simulated (a) ΔT and (b) electrical resistance of a cuboid TEG as a function of aspect ratio (l/A) when the hot-side temperature is varied from 700 K to 850 K.

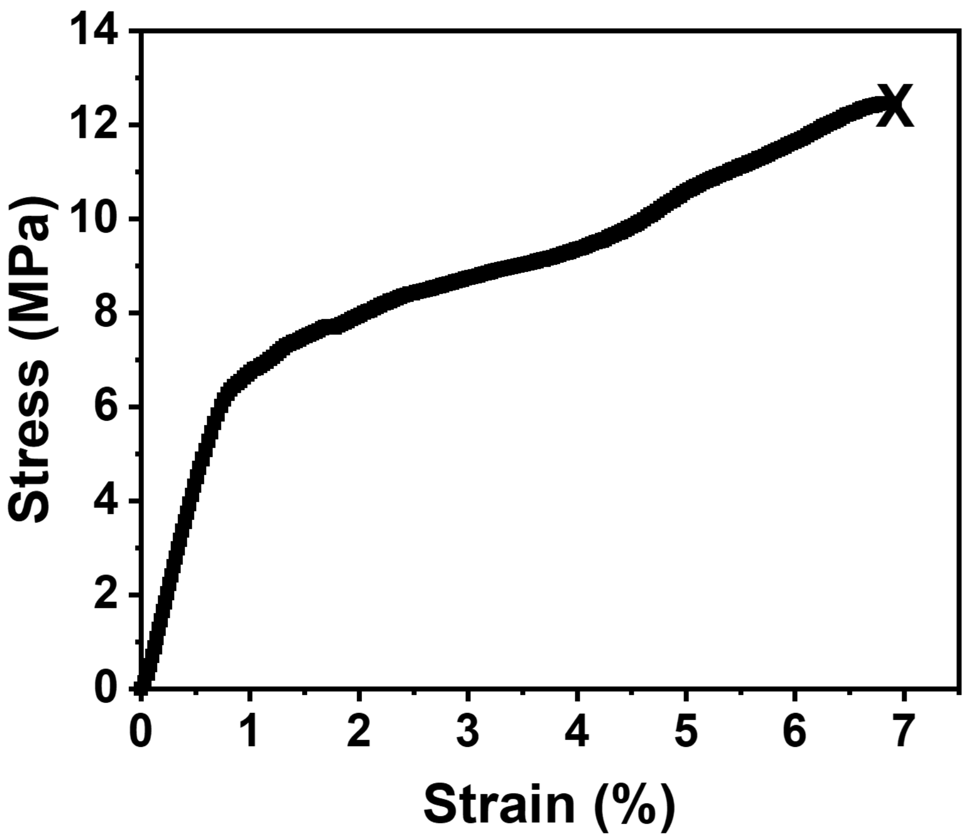

Supplementary Fig. 3 Stress-strain curves of 3D-printed Cu_2Se cuboid by compressive stress test.

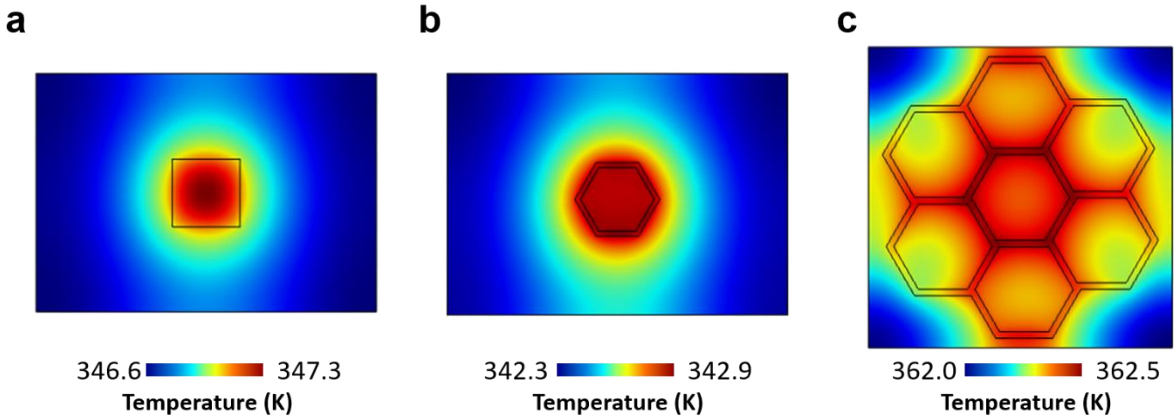

Supplementary Fig. 4 Simulated cold-side temperature distributions of (a) cuboid-, (b) hollow hexagonal column-, and (c) honeycomb-shaped Cu_2Se TE legs when the hot-side temperature is 873 K.

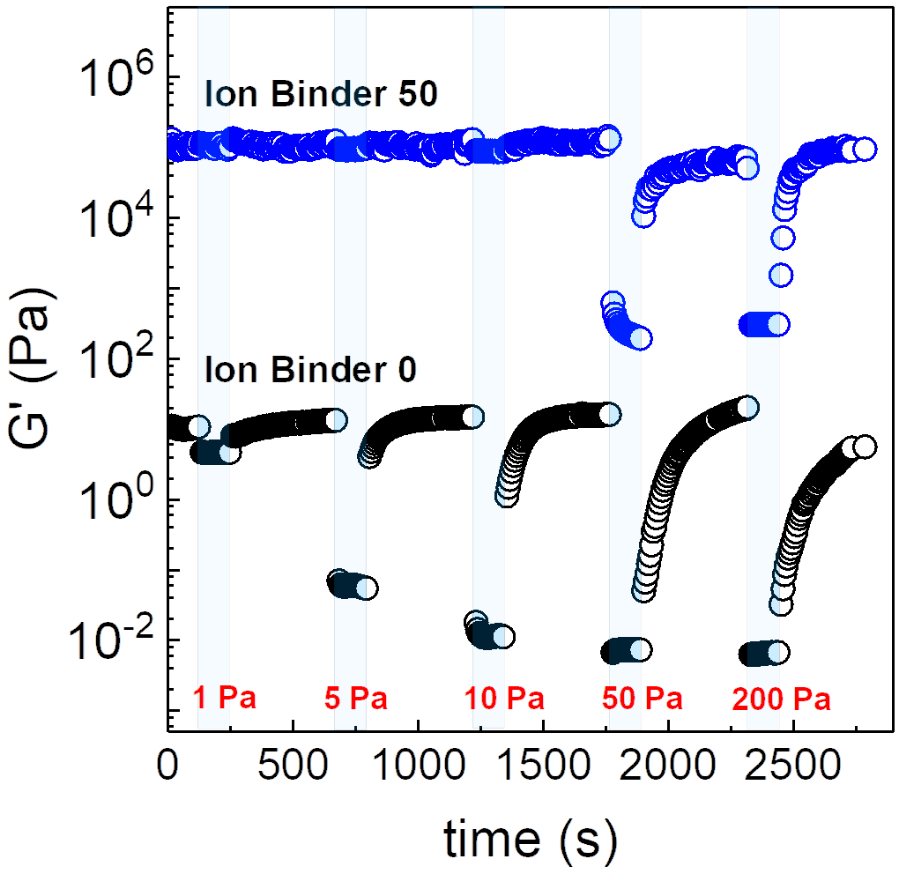

Supplementary Fig. 5 The G' curves from the sequential 3ITTs for binder-free (black symbol) and 50 wt% Se_8^{2-} polyanion binder containing inks (blue symbol) at various shear stresses.

a

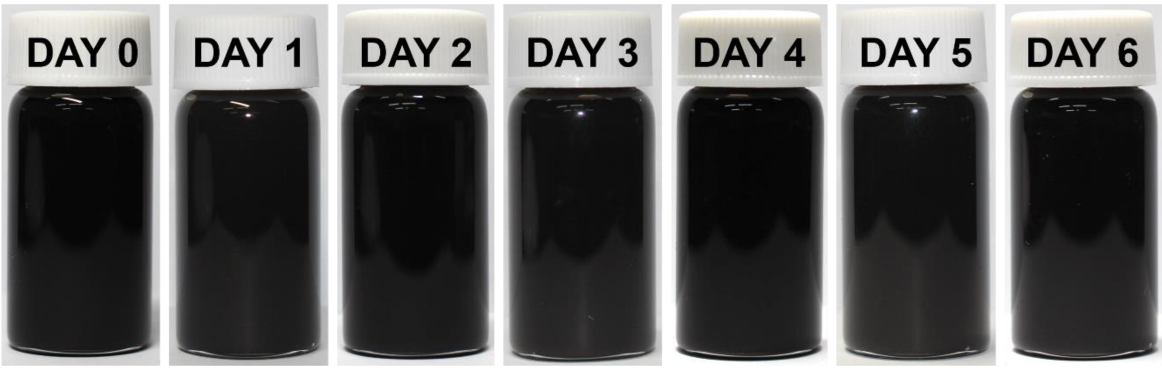

b

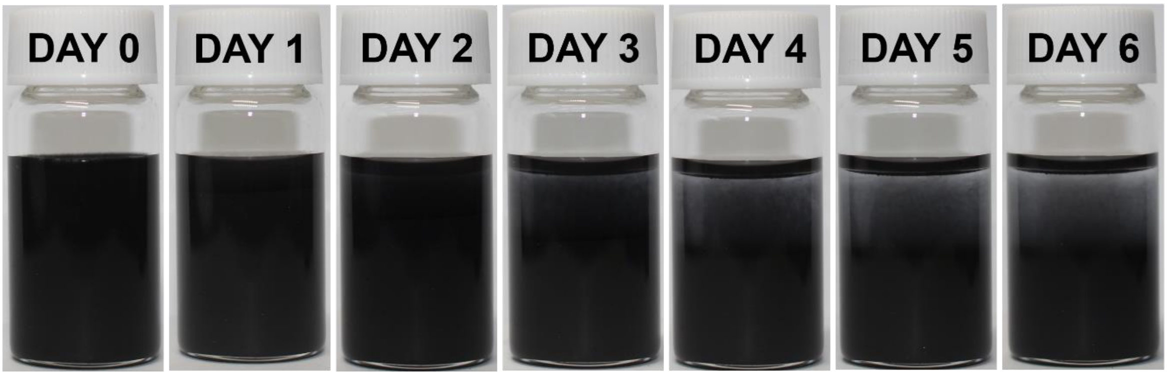

Supplementary Fig. 6 Photographs showing the time-evolution of the dispersibility of Cu_2Se inks (a) with 50 wt% of Se ion binder and (b) without binder inks.

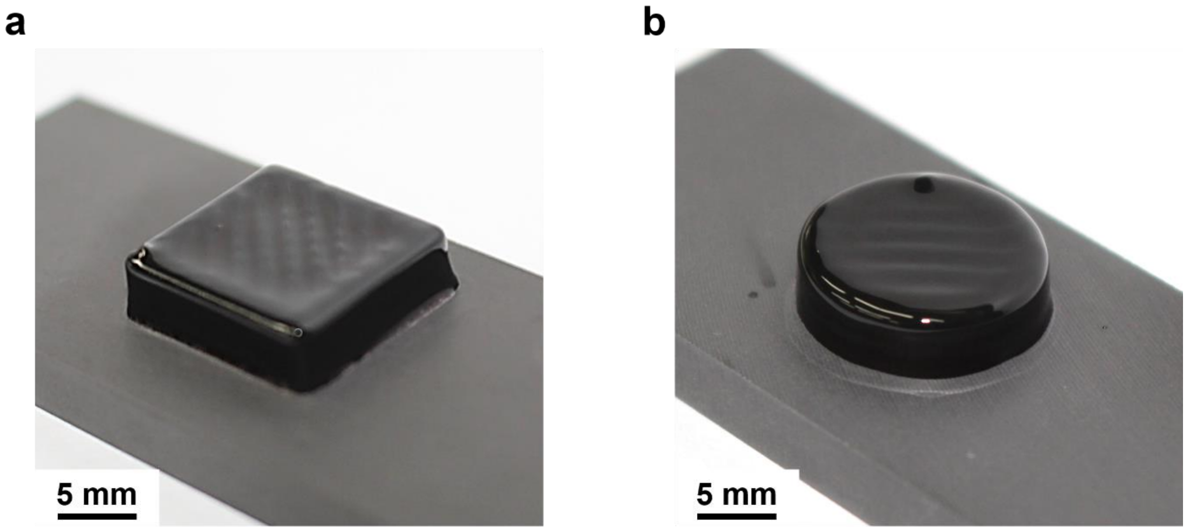

Supplementary Fig. 7 Photographs of the 3D-printed (a) cuboid-and (b) disc-shaped Cu_2Se samples.

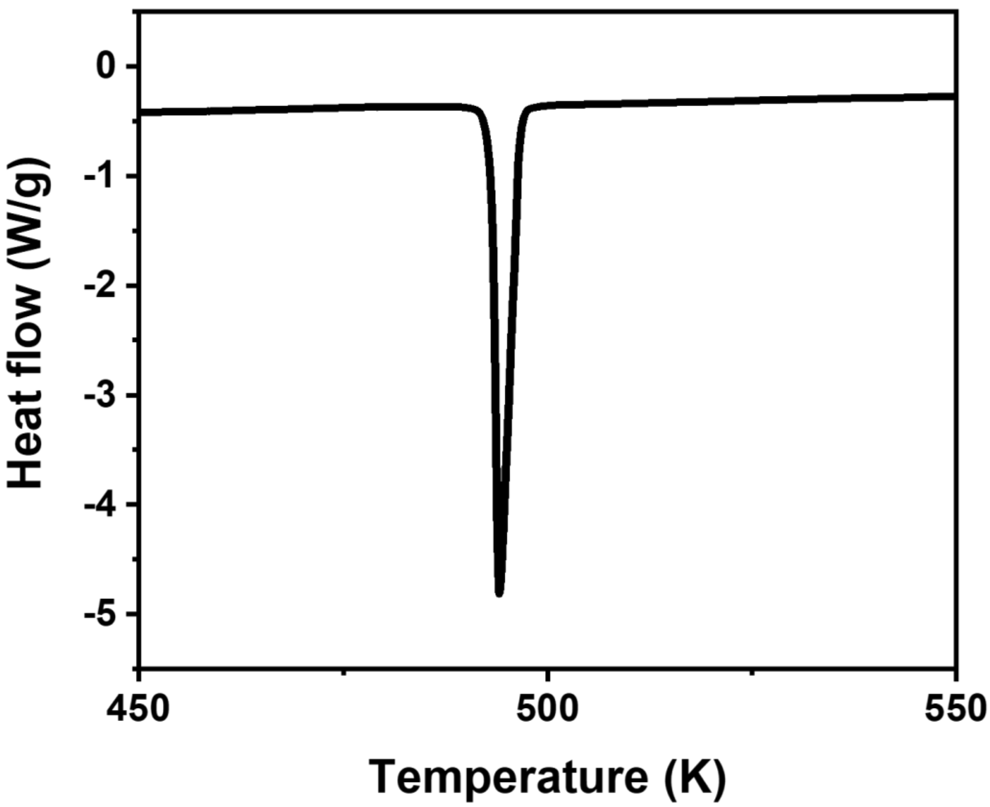

Supplementary Fig. 8 DSC spectrum of the Cu_2Se-based ink.

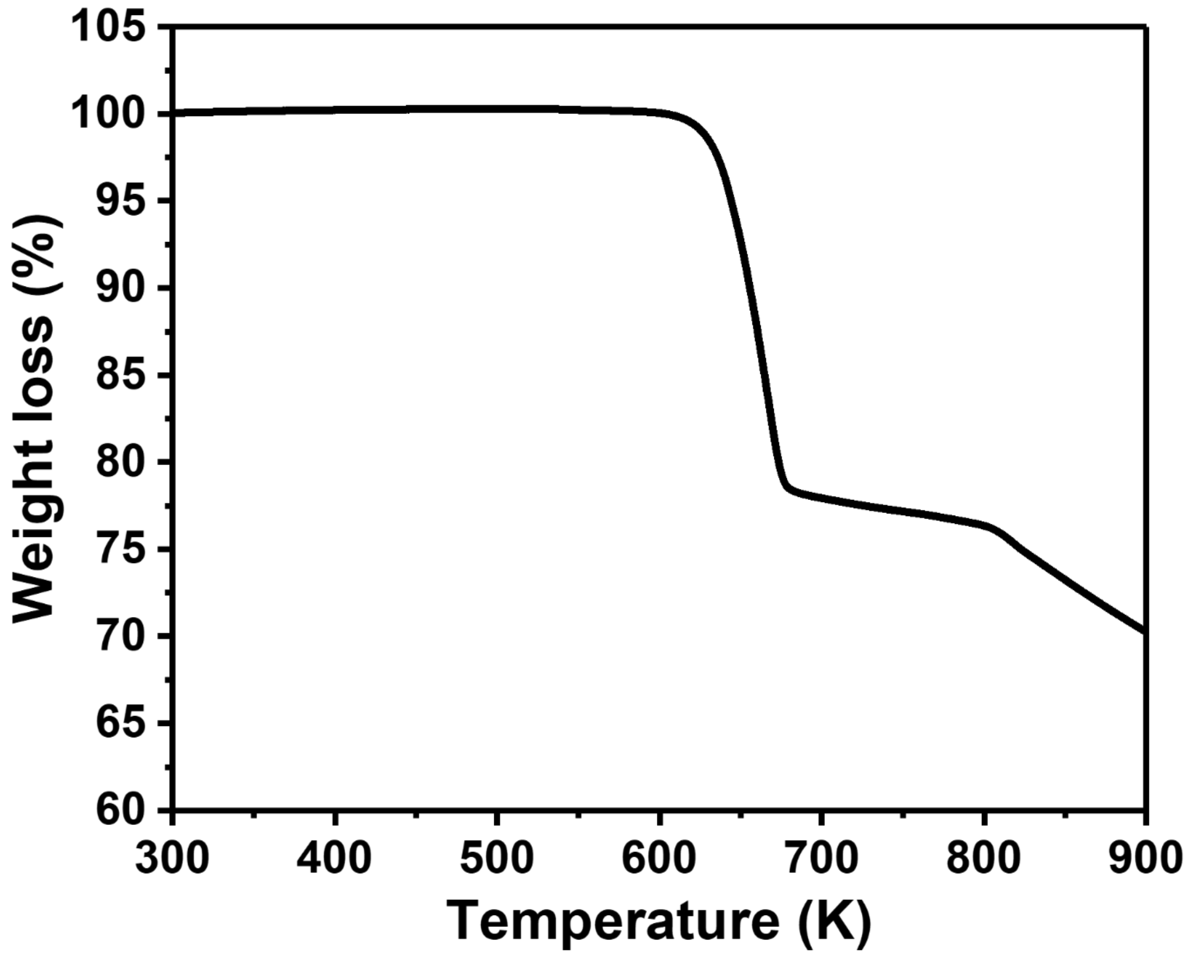

Supplementary Fig. 9 TGA spectrum of a dried Se_8^{2-} polyanion added Cu_2Se ink.

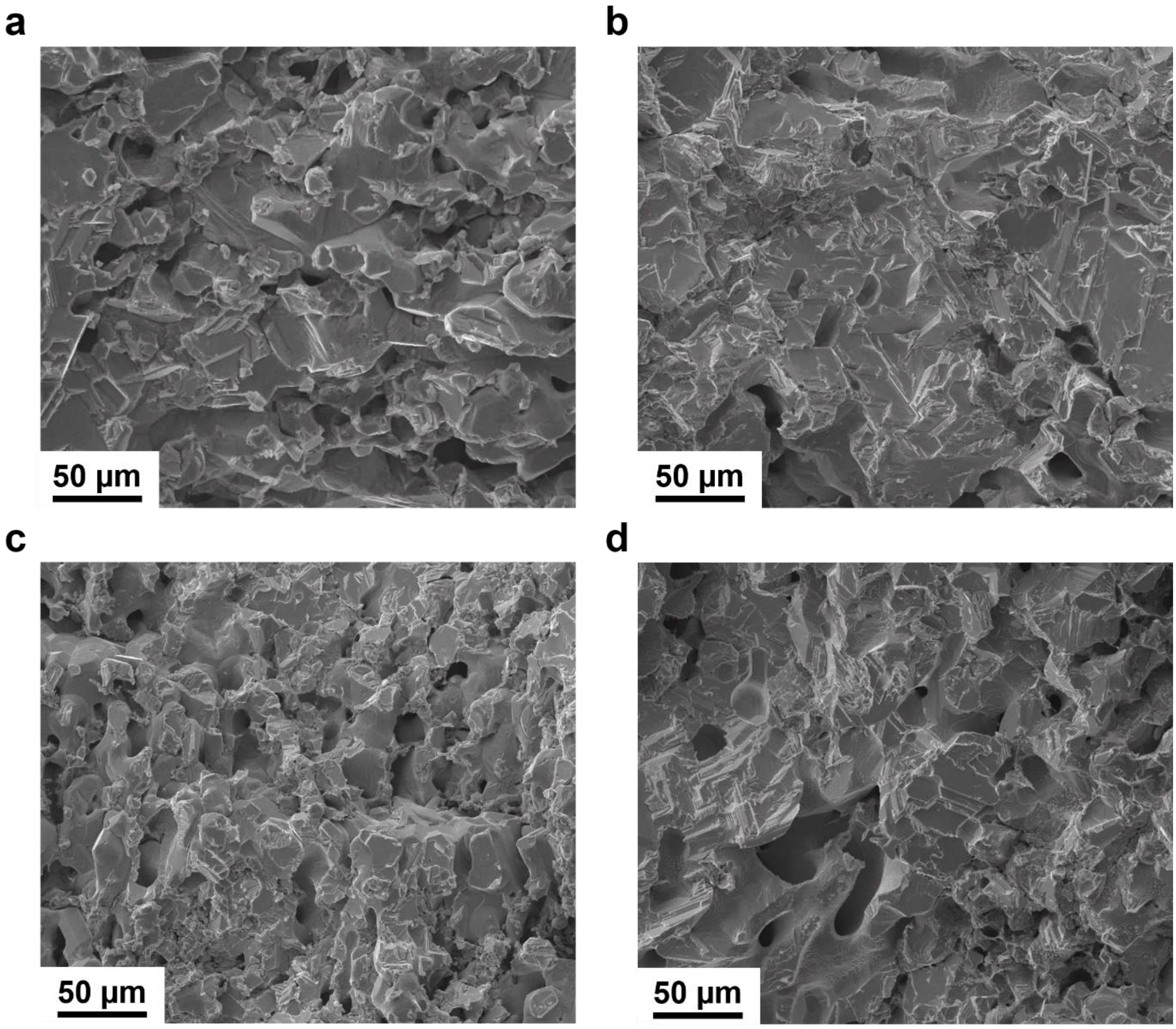

Supplementary Fig. 10 SEM images of 3D-printed $Cu_{2-x}Se$ samples sintered for (A) 1 h, (B) 3 h, (C) 5 h, and (D) 7 h at 873 K.

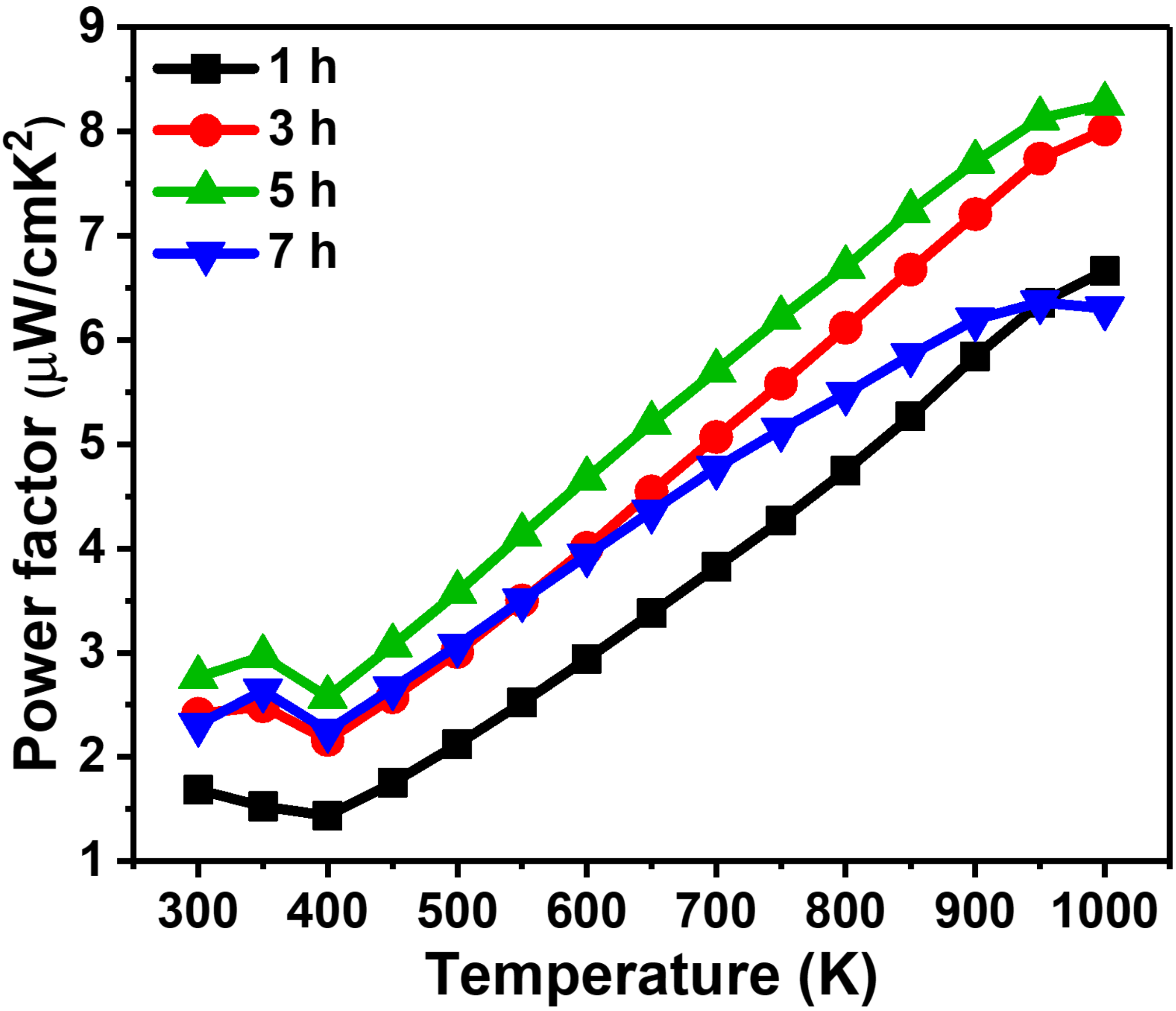

Supplementary Fig. 11 Temperature-dependent power factors of 3D-printed Cu_2Se samples sintered at 873 K for 1, 3, 5, and 7 h.

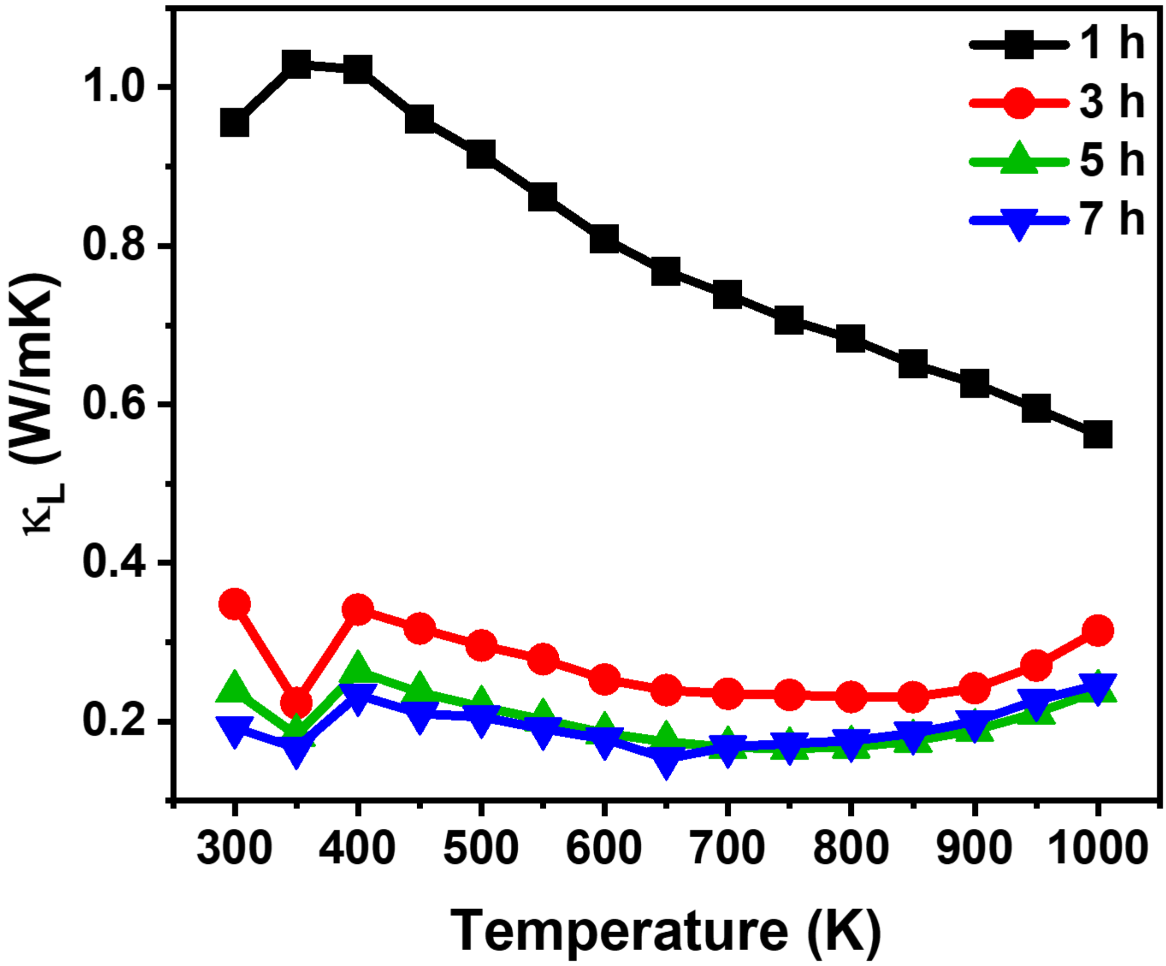

Supplementary Fig. 12 Temperature-dependent lattice thermal conductivities of 3D printed Cu_2Se sintered at 873 K for 1, 3, 5, and 7 h.

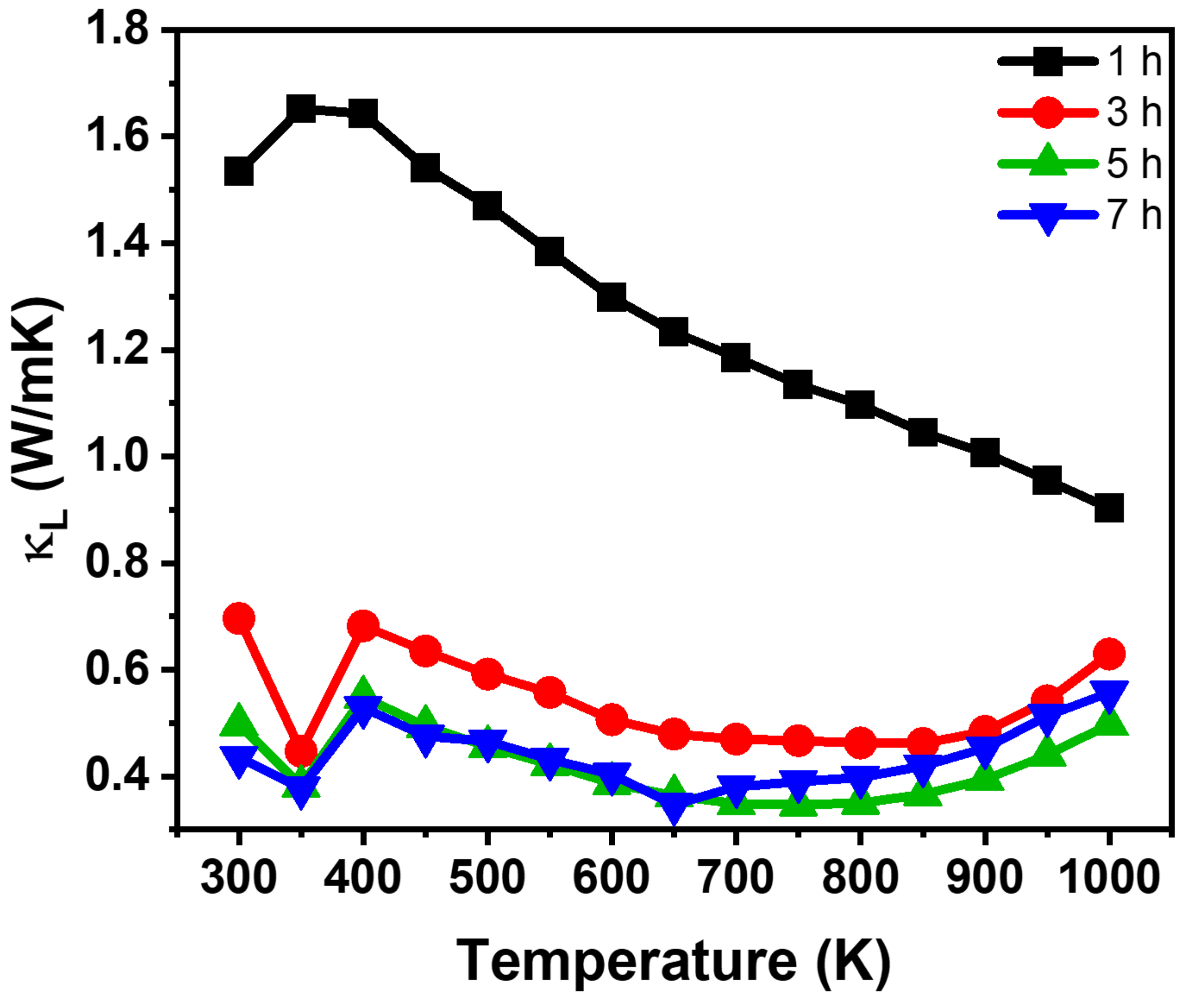

Supplementary Fig. 13 Estimated lattice thermal conductivities of the 100% dense, 3D-printed Cu_2Se sintered at 873 K for 1, 3, 5, and 7 h using the formulation of the modified effective medium theory.

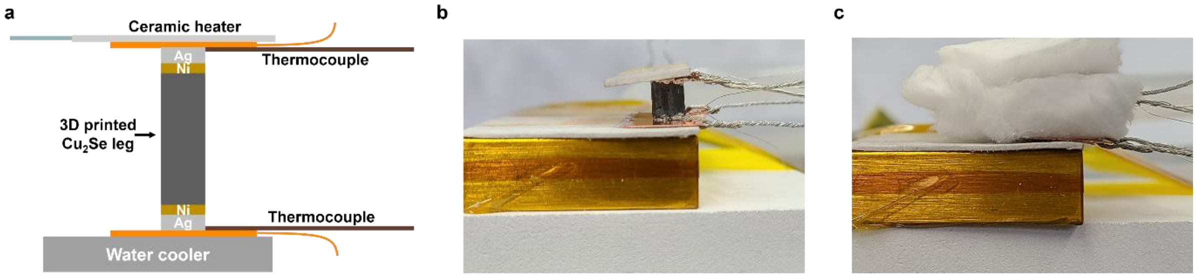

Supplementary Fig. 14 (a) Scheme and photograph showing the output power measurement set-up (b) unveiled and veiled (c) with glass fabric.

Supplementary Table 1. Densities of the 3D-printed $Cu_{2-x}Se$ samples sintered at 873 K for 1, 3, 5, and 7 h.

	1 h	**3 h**	**5 h**	**7 h**
Density (g/cm^3)	**4.89**	**4.10**	**3.97**	**3.71**